Journal of Medical Imaging

MedicalImaging.SPIEDigitalLibrary.org

Reproducing two-dimensional mammograms with three-dimensional printed phantoms

Andreu Badal
Matthew Clark
Bahaa Ghammraoui

SPIE.

Andreu Badal, Matthew Clark, Bahaa Ghammraoui, "Reproducing two-dimensional mammograms with three-dimensional printed phantoms," *J. Med. Imag.* **5**(3), 033501 (2018), doi: 10.1117/1.JMI.5.3.033501.

Reproducing two-dimensional mammograms with three-dimensional printed phantoms

Andreu Badal,[a,*] Matthew Clark,[b] and Bahaa Ghammraoui[a]
[a]U.S. Food and Drug Administration, Center for Devices and Radiological Health, Office of Science and Engineering Laboratories, Division of Imaging, Diagnostics and Software Reliability, Silver Spring, Maryland, United States
[b]University of Maryland College Park, Department of Mechanical Engineering, College Park, Maryland, United States

Abstract. Mammography is currently the standard imaging modality used to screen women for breast abnormalities, and, as a result, it is a tool of great importance for the early detection of breast cancer. Physical phantoms are commonly used as surrogates of breast tissue to evaluate some aspects of the performance of mammography systems. However, most phantoms do not reproduce the anatomic heterogeneity of real breasts. New fabrication technologies, such as three-dimensional (3-D) printing, have created the opportunity to build more complex, anatomically realistic breast phantoms that could potentially assist in the evaluation of mammography systems. The reproducibility and relative low cost of 3-D printed objects might also enable the development of collections of representative patient models that could be used to assess the effect of anatomical variability on system performance, hence making bench testing studies a step closer to clinical trials. The primary objective of this work is to present a simple, easily reproducible methodology to design and print 3-D objects that replicate the attenuation profile observed in real two-dimensional mammograms. The secondary objective is to evaluate the capabilities and limitations of the competing 3-D printing technologies and characterize the x-ray properties of the different materials they use. Printable phantoms can be created using the open-source code introduced, which processes a raw mammography image to estimate the amount of x-ray attenuation at each pixel, and outputs a triangle mesh object that encodes the observed attenuation map. The conversion from the observed pixel gray value to a column of printed material with equivalent attenuation requires certain assumptions and knowledge of multiple imaging system parameters, such as x-ray energy spectrum, source-to-object distance, compressed breast thickness, and average breast material attenuation. To validate the proposed methodology, x-ray projections of printed phantoms were acquired with a clinical mammography system. The quality of the printing process was evaluated by comparing the mammograms of the printed phantoms and the original mammograms used to create the phantoms. The structural similarity index and the root-mean-square error were used as objective metrics to compare the two images. A detailed description of the software, a characterization of the printed materials using x-ray spectroscopy, and an evaluation of the realism of the sample printed phantoms are presented. [DOI: 10.1117/1.JMI.5.3.033501]

Keywords: mammography; breast phantoms; three-dimensional printing.

Paper 17353PRR received Dec. 5, 2017; accepted for publication Jun. 6, 2018; published online Jul. 12, 2018.

1 Introduction

Mammography is the imaging modality most commonly used in clinical practice to screen women for breast abnormalities, and it is a key tool for early detection of breast cancer. Since mammography uses ionizing radiation that might be harmful for the patient, it is essential to minimize the radiation used and balance the risk associated with the exposure with the corresponding medical benefit of the examination. The minimization of the radiation is especially important when screening asymptomatic women that are less likely to obtain a direct benefit from the examination compared to patients that have symptoms of disease.

Given that the exposure of patients to radiation has to be kept as low as possible, physical phantoms are commonly used as surrogates of breast tissue to evaluate some aspects of the performance of new mammography systems and as a quality control measure for existing systems. The majority of physical phantoms used to evaluate mammography are built with uniform blocks of material and do not reproduce the anatomic heterogeneity observed in real breasts. Furthermore, the phantoms typically have a fixed shape and an average attenuation that do not reproduce the great variability in size and composition among different women. Some heterogeneous breast phantoms have been developed in the past.[1,2] Of particular interest is the phantom created in 1990 by Caldwell and Yaffe.[3] This phantom, commercialized by the name of "Rachel phantom," closely reproduces the attenuation profile of a real mammogram using a combination of a carefully carved tissue-equivalent material block for the low-frequency information and a mercury-doped film for the high-resolution information. The mammographic projection of this phantom is similar to a real mammogram, but it represents only the anatomy of a single patient. The complexity in manufacturing this physical phantom limited the

*Address all correspondence to: Andreu Badal, E-mail: andreu.badal-soler@fda.hhs.gov

2329-4302/2018/$25.00 © 2018 SPIE

adoption of this methodology for phantom development. At the time the phantom was built, additive manufacturing technologies that are now becoming available in medical research facilities[4] had not been created.

In this work, we present a simple, easily reproducible methodology to create patient-specific breast phantoms from clinical mammograms using the capabilities of current three-dimensional (3-D) printing technology. The presented tools are not directly applicable to volumetric imaging modalities, such as tomosynthesis or breast CT, but they might be useful in the technical evaluation of two-dimensional (2-D) mammography systems. The three main objectives addressed in this work are to: (1) develop a methodology (and associated software) to design and print 3-D objects that replicate the attenuation profile observed in clinical 2-D mammograms, (2) characterize the x-ray properties of the material used by the 3-D printer used in this work, and (3) estimate the realism of the x-ray projections of the printed phantoms and discuss the potential use of these projections for system performance evaluation.

2 Materials and Methods

2.1 *Computer Software*

A new open-source Python program, called "mammoreplicator," is introduced in this work. The mammoreplicator source code can be downloaded at the website https://github.com/DIDSR/mammoreplicator. The purpose of this software is to create a printable 3-D object that replicates the attenuation seen in a clinical mammogram. The program requires as an input a standard DICOM 2-D mammography image and then produces as an output a 3-D triangle mesh object that encodes the observed attenuation of the original breast. The input mammogram has to provide the unprocessed, raw imaging data (image "for processing"). A mammogram postprocessed "for presentation" is not suitable because it includes logarithmic scaling, flattening of the breast contour, and other image processing steps that are not considered by the current software. The generated triangle mesh is stored in the generic polygon (PLY) format, which can be easily converted to the popular stereolithography (STL) format used by most printers. It is important to note that this software is based on 2-D mammography and is not intended to create anatomically accurate 3-D breasts, as done by other authors.[2]

The foundation of the software is the fact that the gray level of each pixel in the image provides information on the radiological thickness of the breast in the direct path from the x-ray source focal spot to the pixel. Knowing the differences in x-ray attenuation between breast tissues and 3-D printing materials, the observed radiological thickness in a pixel can be converted into a thickness of printed material that will produce an equivalent amount of x-ray attenuation. Therefore, each pixel in the image is transformed into a column of the appropriate height focused to the known location of the x-ray focal spot. Focusing the columns toward the focal spot is important to make sure that the column is projected into a single pixel and not smeared into a line of pixels. This approach to physical phantom development for radiographic imaging is similar to the approach described by Caldwell and Yaffe.[3] Previous works have described sophisticated methods to estimate the thickness of adipose and glandular tissue that are projected into a pixel.[5] The implemented algorithm uses a simpler conversion method that requires knowledge of the x-ray energy spectrum, compressed breast thickness, and average breast material attenuation. As a result of the 2-D to 3-D transformation method, phantoms created by mammoreplicator might not exactly reproduce the anatomic features and contrast from the original mammogram if they are imaged with acquisition parameters different than those specified in the generation of the triangle mesh object. Obviously, the objects will not have any utility for evaluating volumetric imaging modalities, such as tomosynthesis or breast CT, or for ultrasound and MRI studies. Since only the linear attenuation coefficient of x-rays is considered by the software, the scatter produced by the objects will not be representative of the actual 3-D organ. The scatter, quantum and electronic noise, and blurring due to the detector modulation transfer function in the original mammogram are intrinsically included in the 3-D printed object. The unwanted extra scatter produced by the printed object can be evaluated using triangle mesh-based Monte Carlo simulations[6] and subtracted from the triangle mesh model before printing. However, the effect of the antiscatter grid used during the image acquisition has to be taken into account.

The contents of the header section of an example PLY triangle mesh file created by mammoreplicator are shown in Table 1. The input data provided by the user to create the object are stored as comments in the header section. This particular PLY file header also specifies that this triangle mesh is composed of 2,848,192 vertices and 2,850,652 triangles. More triangles than vertices are defined because each vertex is shared by multiple adjacent triangles.

2.2 *Objet Three-Dimensional Printer*

Multiple competing 3-D printing technologies with different strengths and limitations are currently available. The first step in the development of the 3-D printed phantoms was to determine the optimal printer to be used in this application. In a preliminary presentation of this work,[7] we compared the performance of three printers available in our institution based on three different printing technologies: stereolithography, fused deposition modeling, and inkjet printing. The conclusion of this initial study was that the inkjet-based Objet260 Connex3 printer from Stratasys Ltd.,[8] shown in Fig. 1, provided the best combination of reliable operation and high resolution. The nominal printing resolution of this printer is 600 dpi in the x- and y- axes, and 1600 dpi in the z-axis, which, according to the manufacturer, produces a maximum accuracy of 16 μm in the z-axis and 200 μm in the x- and y-axes. The effective printing resolution, or smallest resolvable detail, in our particular application is analyzed in the following section. An additional advantage of this printer is that it has a build plate large enough ($25.5 \times 25.2 \times 20.0$ cm) to print two complete breast phantoms in a single job. Only the results obtained with the Objet printer are presented in this paper for brevity.

2.3 *Effective Printer Resolution Estimation*

To print the virtual 3-D objects produced by mammoreplicator, the physical limitations of the 3-D printer have to be taken into consideration. The most obvious limitation is that the printer cannot print objects at the same resolution as the pixel size of modern mammography detectors. Most mammography systems have a pixel size of the order of 100 μm, but systems with pixels as small as 50 μm exist. Furthermore, due to the magnification effect, the phantom features would need to be even smaller than the pixel size to be unnoticeable. Therefore, in practice,

Table 1 Header section of an example PLY triangle mesh file created by mammoreplicator, showing the input parameters used to create the 3-D mesh from the 2-D DICOM mammogram.

```
ply

format ascii 1.0

comment ** 3-D geometry in STL format created by
mammoreplicator.py from file:

comment. /CancerImaging_TCGA-BRCA_TCGA-A0-A0JB_
Dig-Diag-Mammo_Raw_3.dcm

comment

comment – Input conversion parameters
(Tue Feb 2 13:12:19 2016)

comment compression_thickness = 6.0

comment average_breast_intensity = 800

comment air_intensity = 16383

comment mfp_breast = 1.284

comment mfp_plastic = 1.284

comment center_pixel = [0 0]

comment center_coord = [0 0 0]

comment source_coord = [0 10.7828286 66]

comment pixel_size = 0.0094091

comment output_binning = 3

comment binned columns = 466, binned rows = 764

comment

element vertex 2848192

property float x

property float y

property float z

element face 2850652

property list uchar int vertex_index

end_header
```

the clinical mammograms need to be downsampled to produce printable objects, even if this process reduces the high-frequency information available in the projections of the printed objects. The minimum downsampling of the mammograms required to produce printable phantoms depends on the resolution of the printer.

Since the physical phantoms produced in this work are composed essentially of thin tilted columns, a method to evaluate the smallest column size printable in a given printer was developed. A test object was created from a 1-cm^2 region of interest (ROI) inside an example mammogram with 100-μm pixels. The pixels in the ROI were rebinned (downsampled) in groups of 2×2, 3×3, 4×4, 5×5, 6×6, 7×7, and 8×8 pixels. The triangle

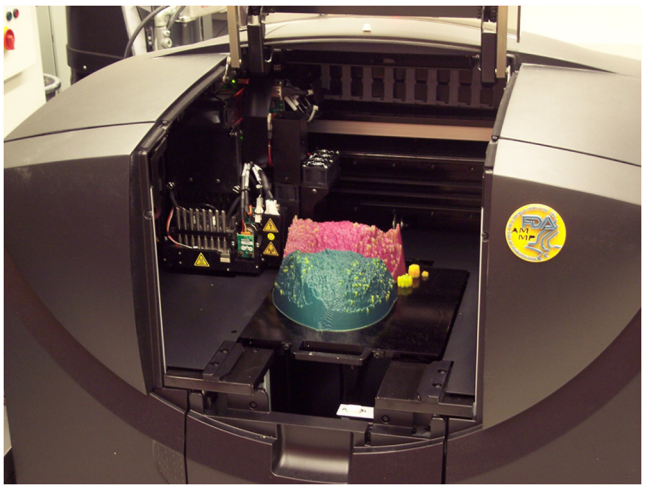

Fig. 1 Picture of the inkjet-based Objet260 Connex3 3-D printer from Stratasys Ltd. used to print the mammography phantoms. Two recently printed phantoms can be seen on the build plate. The printer deposited yellow support material above the phantom to assist in the printing of the tilted columns.

meshes generated from the full-resolution ROI and the rebinned ROIs had columns with widths between 100 and 800 μm. The test object incorporated the eight ROIs at decreasing resolutions and a line of cylinders of decreasing diameters for reference. The virtual triangle mesh of the test object and two example prints of the object are shown in Fig. 2. Evaluating the quality of the printed columns, it was determined that for the tested printers the optimal rebinning was 3×3. Below 3×3, the printed columns did not reproduce correctly the triangle mesh, and some printing artifacts were visible.

2.4 *Printed Material Characterization*

The x-ray attenuation properties of the proprietary material used by the tested 3-D printer were experimentally characterized. The mean x-ray attenuation of the material for the x-ray energy spectrum that will be used to image the phantom is one of the parameters that have to be input to mammoreplicator. This parameter has a direct effect on the height of the columns that are created to reproduce the attenuation seen in the mammogram. Highly attenuating materials will require shorter columns than less attenuating materials. The possibility to use any single material to print the phantoms is an important advantage of the phantom development method presented in this work, because there are few printers that can use multiple materials, and, to our knowledge, there is not any printing material currently available with the low x-ray attenuation of adipose tissue. The variable column length produces the desired attenuation of the primary beam at each pixel, but the user has to be aware that the scatter coming from the phantom will not reproduce the scatter produced by the real tissue (especially the coherent scattering component).

One possible method to estimate the effective x-ray attenuation of a 3-D printer material consists in acquiring an x-ray projection of a step phantom. Knowing the step thickness and the corresponding pixel gray level, it is possible to estimate the mean attenuation coefficient for the used energy spectrum using the exponential attenuation equation. However, with this method, we would not be able to estimate the material attenuation at energy spectra different than the one used in the image

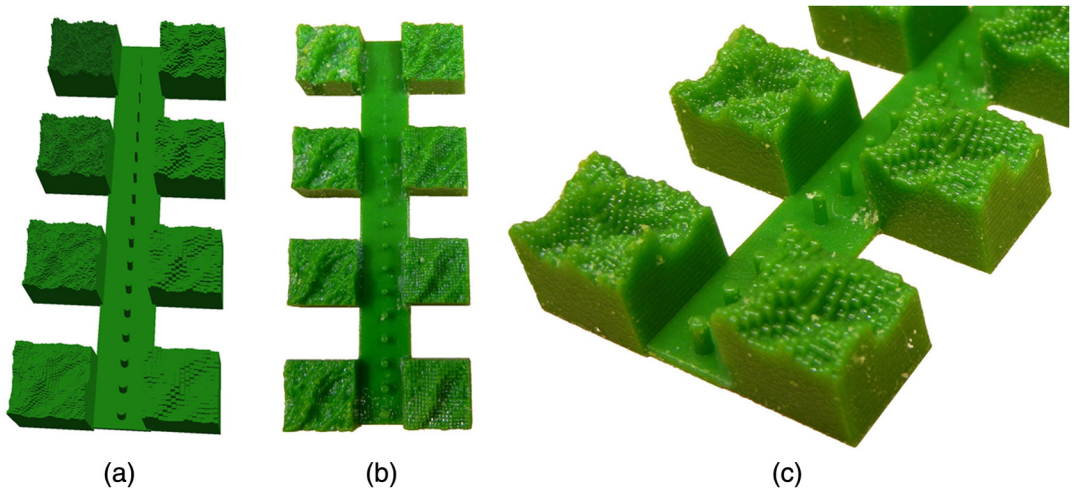

Fig. 2 Test object used to evaluate the effective printer resolution in our application. This object was constructed using a 1-cm^2 ROI from a real mammogram. Eight copies of the ROI rebinned to produce column widths between 100 and 800 μm were printed together, along with a series of cylinders with decreasing diameter. (a) Rendering of the test object STL triangle mesh, (b) printout of the test object with the Objet260 Connex3 printer (support material residue can be seen at the highest resolution region), and (c) close-up of the printed object.

acquisition. To be able to build phantoms that will display the required pixel contrast at other given x-ray energies, the material attenuation coefficient spectrum as a function of energy was measured using a cadmium telluride (CdTe) spectroscopic detector.

2.5 *Comparison of Clinical and Phantom Images*

The key element that will determine the utility of the proposed phantom development process is the ability of the phantoms to transfer the anatomical information shown in the original patient mammograms to new mammograms acquired with the phantoms instead of the patients. Multiple sources of variability can affect the transfer of information, such as the approximations used in the transformation of the 2-D image to a 3-D mesh object, and the intrinsic limitations of the 3-D printing process and the new image acquisition process (with the added blur and noise). To evaluate the accuracy of the x-ray projections of the printed phantoms, the phantoms were imaged in a clinical mammography system (Hologic LORAD Selenia system, Hologic Inc., Marlborough, Massachusetts). The images were acquired with a 28-kVp, molybdenum target, spectrum using the standard antiscatter grid, and the default automatic exposure parameters for screening mammography. A source-to-object distance of 66 cm was used, which is the distance used as an input parameter in the creation of the phantoms. The original mammograms were acquired in an imaging system that had some technical and geometrical differences to the one used with the phantoms, such as different pixel sizes, energy spectra, magnification, and object orientation. For this reason, it was not expected that the two images would be identical down to the individual pixel level. To perform a fair comparison of the two images and correct for the distortions in contrast (due to different spectra), size (due to magnification), and orientation (due to misalignment) of the anatomical features, the phantom images were rescaled and registered to the original images using the automated image registration tools available in MATLAB's Image Processing toolbox (MathWorks, Inc., Natick, Massachusetts). The primary figure of merit that we used to compare the similarity between the original and phantom images was the structural similarity index[9] (SSI). The mean square error (MSE) is an alternative metric commonly used to estimate signal fidelity, but it is known to perform poorly in some image perception tasks.[10] One of the main limitations of the MSE is that it relies only on individual pixel values, and it does not take into account the pixel correlations that are important for image interpretation by the visual system. Therefore, the MSE results depend strongly on the image registration algorithm, and images with a lower or higher MSE might not correlate to images considered more or less similar by a human observer. (For example, a constant pixel shift or offset in the gray-level values will result in a large MSE, but the differences might be unnoticeable by an observer.) In addition, the MSE values are not set in a finite scale and there is not a clear way to interpret the degree of similarity between two images from an isolated MSE value. In contrast, the SSI is a metric that has been shown to compare well with observers ranking the similarity of images, and its finite scale (with 1 meaning identical images) enables the interpretation of degree of image similarity with a single measurement. As originally defined by Wang et al.,[9] the SSI metric evaluates the similarity of two images, or parts of the image, combining three separate features: luminance, contrast, and structure. These features are computed based on the mean pixel value (luminance), the pixel standard deviation (contrast), and the pixel cross correlation (structure). In this work, the structural similarity was computed using the corresponding function from MATLAB's Image Processing toolbox. The use of objective figures of merit to characterize the similarity of the original and phantom images allows not only to estimate the realism of the phantom but also provides a useful method to compare the accuracy of different printers or printing parameters.

3 Results and Discussion

3.1 *Material Characterization*

The results of the characterization of the Objet printed material with the x-ray spectroscopy detector are shown in Fig. 3. The

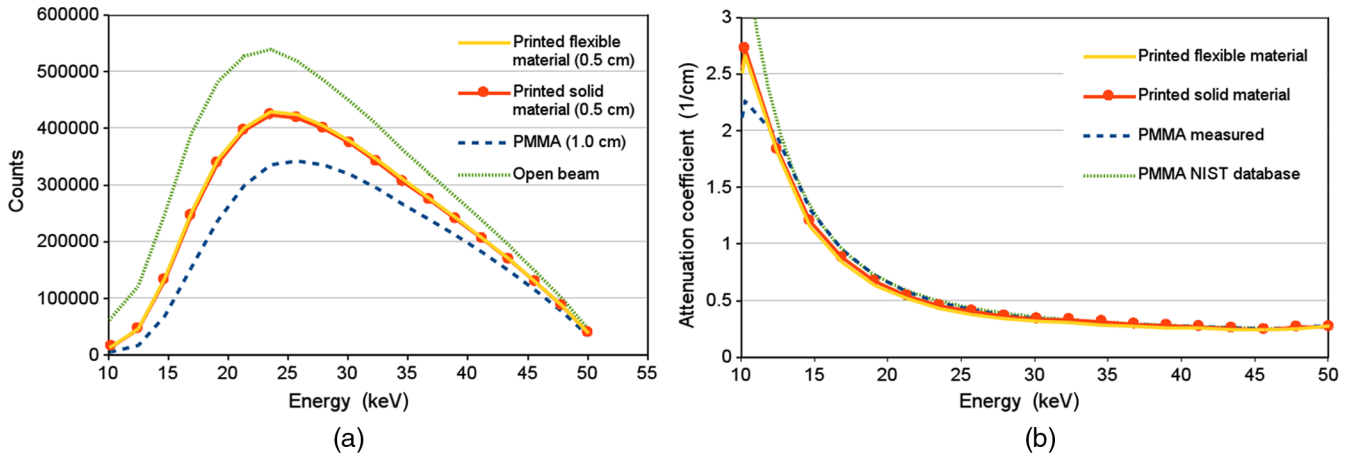

Fig. 3 Measurement of the x-ray attenuation of the flexible (TangoBlackPlus) and solid (VeroMagenta) Objet 3-D printer materials: (a) x-ray transmission spectra measured with the CdTe spectroscopy detector, after correction of the detection efficiency, *k*-edge escape, and pile-up and (b) estimated x-ray attenuation coefficient. Measurement of a PMMA sample and the attenuation spectrum of PMMA from an NIST database are provided as reference.

attenuation spectra were measured with an XR-100T CdTe spectroscopic detector from Amptek (Bedford, Massachusetts). The effects of the limited detection efficiency, *k*-edge escape, and count pile-up in the raw spectra were corrected using the simulated system response matrix described by Ghammraoui et al.[11] Two different proprietary printed materials were studied: a flexible material (TangoBlackPlus) and a solid material (VeroMagenta). A polymethyl methacrylate (PMMA) sample was also evaluated as a control. Comparing the results for this control material to its attenuation coefficients published in the National Institute of Standards and Technology (NIST) database, we show that our measurements are accurate for energies above 12 keV. The number of counts below 12 keV was too low to compute reliable results, but x-rays at these low energies are attenuated so efficiently that they do not contribute significantly to the radiographic images. The measurements show that the x-ray attenuation of the two printed materials is very similar, with an average reduction in attenuation for the flexible material of 5% (in the 15- to 30-keV interval) due to its slightly lower density. The attenuation of the solid materials is also on average 5% lower than PMMA between 15 and 30 keV. Using the measured linear attenuation spectrum, we estimated that the printer material has an average x-ray attenuation of 0.89 cm^{-1} for a typical mammography x-ray beam (28 kVp molybdenum source, beam quality RQR-M 2 from IEC 61267:2005).

3.2 *Printed Physical Phantoms*

Three breast phantoms were created using the Objet260 Connex3 printer from three publicly available, anonymized clinical mammograms from "The Cancer Genome Atlas Breast Invasive Carcinoma" collection.[12] The original mammograms were acquired with a GE Senographe DS system with 100-μm pixels. Each phantom required nearly 10 h of printing time. The reliability of this professional printer allowed printing two full-size phantoms at the same time, as shown in Fig. 1. The average weight of the phantoms was 750 g, which corresponds to an approximate raw material cost of $220 for each phantom.

Figure 4 shows an example craniocaudal (CC) mammogram of a fatty breast, the corresponding computational model created by the mammoreplicator software, the physical realization of the

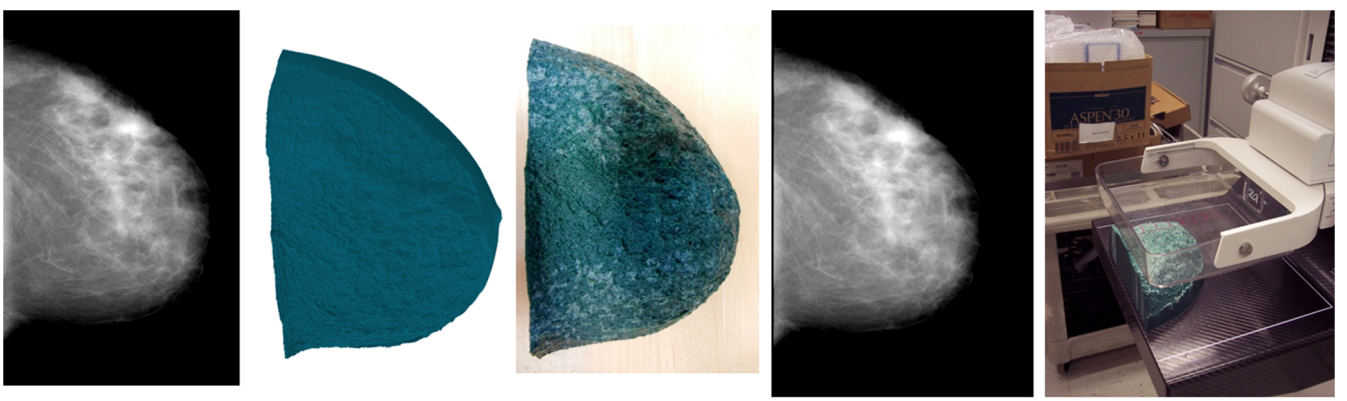

Fig. 4 CC mammography image of a fatty breast and 3-D printed surrogate printed using Stratasys' Objet260 printer with VeroCyan material. (a) Original mammograms, (b) triangle mesh phantom, (c) printed phantom, Objet260 printer, (d) phantom mammogram, and (e) phantom image acquisition.

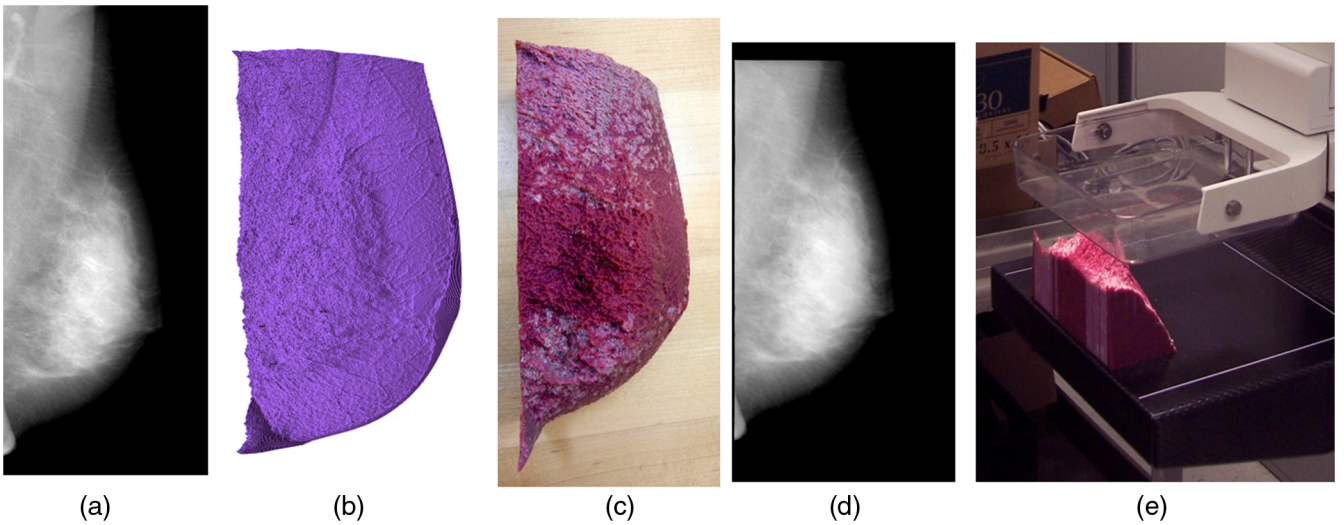

Fig. 5 MLO mammography image of a dense breast and 3-D printed surrogate printed using Stratasys' Objet260 printer with VeroMagenta material. (a) Original mammogram, (b) triangle mesh phantom, (c) printed phantom, Objet260 printer, (d) phantom mammogram, and (e) phantom image acquisition.

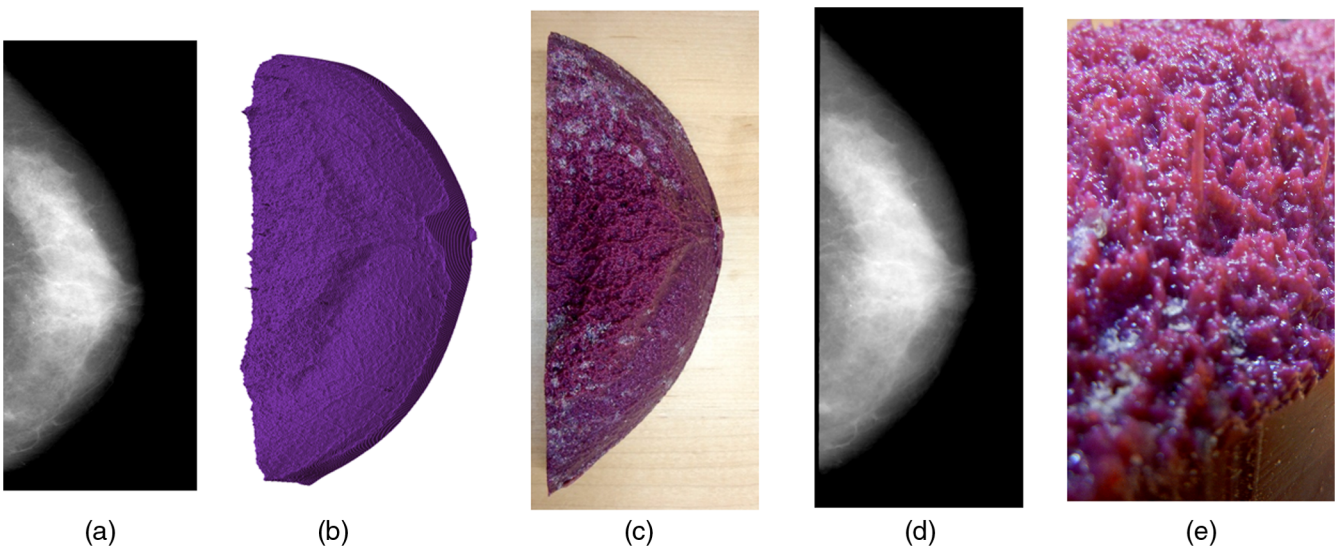

Fig. 6 CC mammography image of a dense breast and 3-D printed surrogate printed using Stratasys' Objet260 printer with VeroMagenta material. (a) Original mammogram, (b) triangle mesh phantom, (c) printed phantom, Objet260 printer, (d) phantom mammogram, and (e) close-up of the phantom surface.

phantom, and an x-ray projection of the phantom acquired in a clinical mammography system. Figures 5 and 6 show the corresponding images for a set of CC and mediolateral-oblique (MLO) mammograms from a patient with dense breasts that was diagnosed with invasive ductal carcinoma. The pictures of the phantoms being imaged in the mammography system show that the breast compression paddle was positioned a few centimeters above the phantoms. Users must be careful to never put pressure on top of the phantom, or some of the printed columns might break.

3.3 *Evaluation of Phantom Images*

The realism of the mammographic projections of the 3-D printed phantoms was evaluated using two methods: first, comparing qualitatively the projections of a clinically relevant ROI of the original mammogram and second, comparing the full-field images using an objective image similarity metric. For the qualitative evaluation, an ROI near the center of the phantom projection shown in Fig. 6(d) was registered to the corresponding ROI in the original clinical mammogram shown in Fig. 6(a). The registered ROI images are displayed side by side in Fig. 7. Since the pixels of the original image were rebinned 3×3 before creating the triangle mesh phantom, the rebinned ROI is provided for comparison. It can be seen that the filament texture of the glandular tissue and the sparse adipose tissue compartments are well replicated in the phantom projection. The phantom projection displays a little more blurring than expected from the rebinned image. This extra blurring can be explained by small geometric inaccuracies in the printing process, misalignment between the phantom and the designed focal spot location, and the intrinsic image blur and noise added by the image

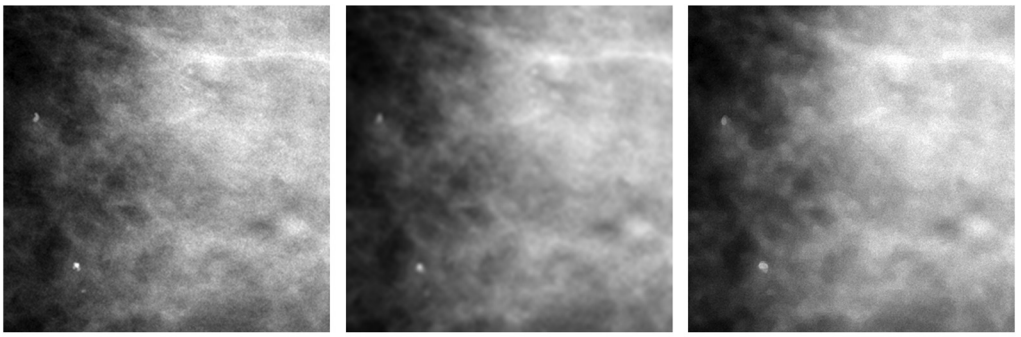

Fig. 7 ROI in the original CC mammography image and registered 3-D printed surrogate. (a) Original mammogram at full resolution (90-μm pixels), (b) original mammogram after 3×3 pixel binning, and (c) mammogram of phantom printed from 3×3 binned data.

acquisition process due to the characteristic modulation transfer function of the x-ray detector. The selected ROI contains multiple microcalcifications, seen as bright white spots in the original image. The two largest microcalcifications are clearly seen in the phantom image, and the contrast is comparable to the contrast seen in the rebinned image. These microcalcifications can be readily seen in the close-up picture of the printed object [Fig. 6(e)] as tall columns extending above the shorter background columns. The columns do not contain any calcium or other high attenuation material, but the longer length of plastic produces the desired increase of x-ray attenuation. The fact that these tall columns are projected as a round dot and not as a line segment demonstrates that the columns were correctly printed at the exact tilt angle to point to the known x-ray focal spot location.

The similarity between the patient mammograms (without rebinning) and the phantom mammograms was objectively evaluated using the structural similarity metric.[9] Figures 8(a) and 8(b) show the original image of the fatty breast patient and the registered phantom image. The comparisons of the two images using a simple pixel-by-pixel relative difference and using the SSI are presented in Figs. 8(c) and 8(d), respectively. Figure 9 shows the SSI maps for the comparison of the original and phantom projections of the dense breast patient. The SSI maps show that, while the pixel relative difference fluctuates as much as 30%, the SSI is very close to unity in large regions of the images, indicating a high degree of similarity in those regions. It is observed that the SSI falls below 0.80 in some of the brightest regions of the images, which correspond to the regions of the breast with the largest attenuation. These regions contain high-resolution glandular tissue structures that might be more affected than other regions by the blurring introduced with the image rebinning. The high-density structures have to be printed as thin, tall columns that are susceptible to inaccuracies in the phantom construction and image acquisition process. The bright regions also have lower pixel values and, therefore, have increased relative noise and might be more affected by scatter coming from other parts of the phantom, which is not accurately reproduced by these phantoms. Table 2 presents the quantitative results of the comparison of the two images, averaged for all the pixels. The results show that the full-field images have an average SSI larger than 0.9,

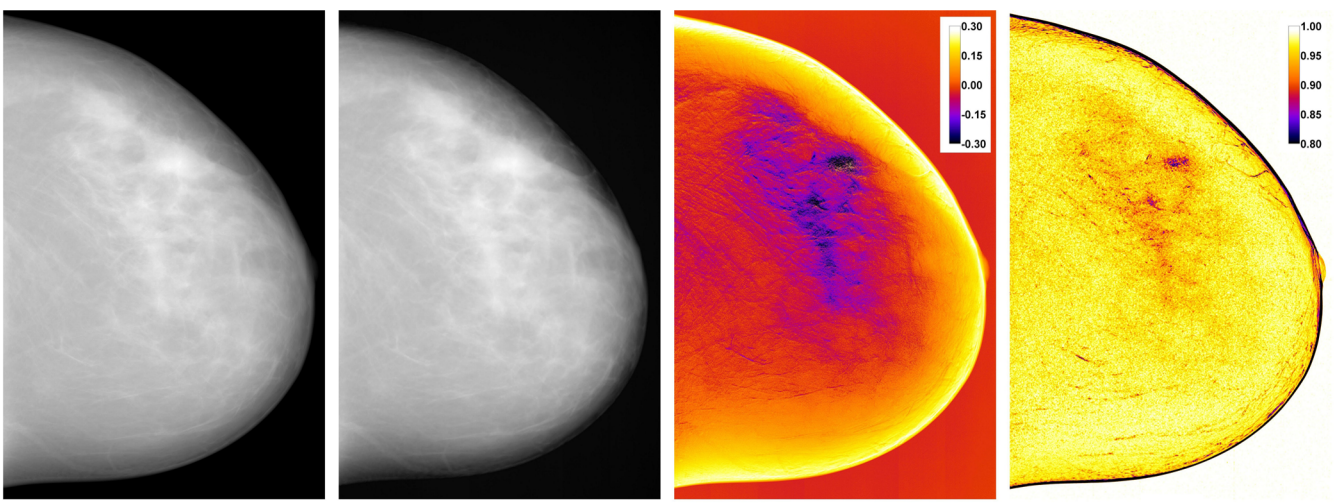

Fig. 8 Evaluation of the similarity of the projection images for the fatty breast shown in Fig. 4: (a) original patient mammogram, (b) phantom mammogram after registration to the original image, (c) relative difference pixel by pixel, and (d) SSI map.

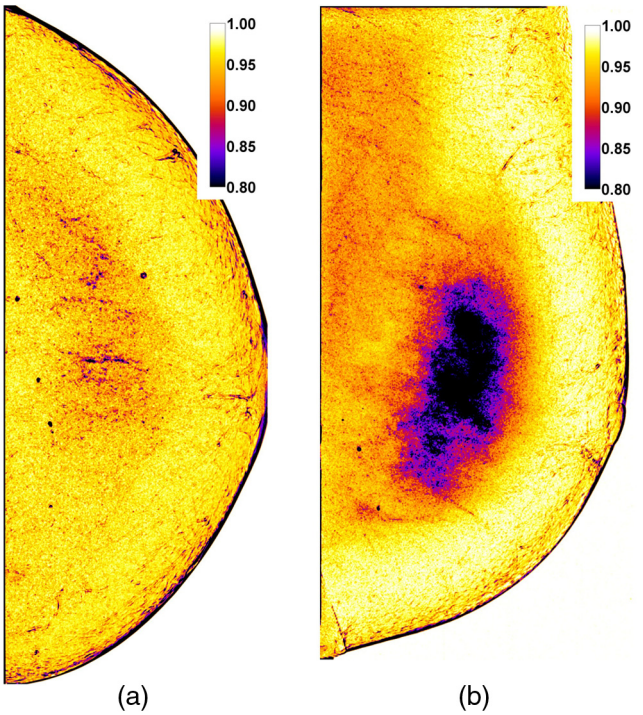

Fig. 9 SSI maps for the two projections of the phantoms created from two views of a patient with dense breast: (a) similarity for the CC view shown in Fig. 6 and (b) similarity for the MLO view shown in Fig. 5.

which indicates a good similarity between the phantom and the original images. Comparing the phantom image with the original image rebinned 3×3, which was used to generate the phantom geometry, produces a small increase in the SSI, as expected. The reported MSE and relative pixel difference show that the two images are far from being identical at the pixel level, even after the registration process. The results provide evidence that the proposed phantom printing methodology can be used to generate phantom images that display the anatomical features found in real patient images, even though the highest resolution details are not reproduced, as expected, due to the limited resolution of the printing process that requires rebinning of the input images. The SSI and MSE measurements will be valuable to objectively quantify the improvement in printing quality in phantoms that we will print in the future using the same input images but different 3-D printers.

Table 2 Comparison of the patient and phantom images using the SSI, the MSE, and the mean pixel relative difference. All comparisons were made with the original high-resolution image, except the third column for which the original image was rebinned in 3×3 pixels.

Phantom	SSI	SSI (3×3 binning)	MSE	Mean pixel relative difference
Fatty CC (Fig. 4)	0.959	0.961	0.0036	0.007
Dense MLO (Fig. 5)	0.944	0.960	0.0033	−0.086
Dense CC (Fig. 6)	0.953	0.954	0.0054	0.065
Dense ROI (Fig. 7)	0.622	0.842	0.0020	0.113

It is worth noting that some of the differences found between the original and phantom images were caused by the fact that the images were acquired with mammography systems from different manufacturers. The differences in automatic exposure control, energy spectra, detector characteristics, and (potentially) image processing between the two systems affected the relative contrast and sharpness of the images. Any discrepancy between the acquisition source-to-phantom distance and the distance defined in the phantom construction process would cause the projection of the tilted columns to spread into line segments on the detector plane, further reducing the image sharpness. Using identical systems would have eliminated this source of uncertainty in the validation. Nevertheless, the observed similarity of the images demonstrates that the fidelity of the phantom projection is not too sensitive to the acquisition parameters, and that the phantoms can generate useful images in different imaging systems.

4 Conclusion

This work shows that 3-D printing technology can be used to produce patient-specific breast phantoms that can be imaged with clinical mammography systems. With the introduced open-source software, researchers can easily create a collection of printed phantoms that reproduce the anatomic variability of real breasts, including varying densities, heterogeneous structures, architectural distortions, and benign and malignant lesions. The 3-D printer evaluated in this work was not able to accurately replicated details in the clinical mammograms below 300 μm. However, features larger than 300 μm were successfully reproduced in the phantoms. A study of the similarity of the original and phantom mammograms demonstrates that the anatomical features were reproduced with good fidelity (mean SSI above 0.9). The mammograms acquired from the printed phantoms show microcalcifications and fibroglandular tissue texture. These images could be used to evaluate aspects of the performance of breast imaging systems that do not rely on the detection of high-resolution features. For instance, multiple phantoms could be imaged regularly as part of the quality control process or could be used to analyze changes in a nonlinear image processing algorithm used to generate mammograms for presentation.

Disclosures

No conflict of interest, financial or otherwise, is declared by the authors.

Acknowledgments

We gratefully acknowledge the assistance of Lynda Ikejimba, PhD, in the acquisition of the phantom images in the clinical mammography system. The phantoms were printed at the Food and Drug Administration's Additive Manufacturing of Medical Products core facility. The results published here are in whole or part based upon data generated by the TCGA Research Network. The mention of commercial products, their sources, or their use in connection with material reported herein is not to be construed as either an actual or implied endorsement of such products by the Department of Health and Human Services.

References

1. A. Carton et al., "Development of a physical 3D anthropomorphic breast phantom," *Med. Phys.* **38**, 891–896 (2011).
2. N. Kiarashi et al., "Development of realistic physical breast phantoms matched to virtual breast phantoms based on human subject data," *Med. Phys.* **42**, 4116–4126 (2015).
3. C. B. Caldwell and M. J. Yaffe, "Development of an anthropomorphic breast phantom," *Med. Phys.* **17**, 273–280 (1990).
4. J. Matsumoto et al., "Three-dimensional physical modeling: applications and experience at Mayo clinic," *Radiographics* **35**, 1989–2006 (2015).
5. S. van Engeland et al., "Volumetric breast density estimation from full-field digital mammograms," *IEEE Trans. Med. Imaging* **25**, 273–282 (2006).
6. A. Badal et al., "penMesh-Monte Carlo radiation transport simulation in a triangle mesh geometry," *IEEE Trans. Med. Imaging* **28**, 1894–1901 (2009).
7. M. Clark, B. Ghammraoui, and A. Badal, "Reproducing 2D breast mammography images with 3D printed phantoms," *Proc. SPIE* **9783**, 97830B (2016).
8. Stratasys, "Objet260 connex3 specification sheet," Technical Report (2016).
9. Z. Wang et al., "Image quality assessment: from error visibility to structural similarity," *IEEE Trans. Image Process.* **13**(4), 600–612 (2004).
10. Z. Wang and A. C. Bovik, "Mean squared error: love it or leave it? A new look at signal fidelity measures," *IEEE Signal Process. Mag.* **26**(1), 98–117 (2009).
11. B. Ghammraoui, A. Badal, and S. Glick, "Feasibility of estimating volumetric breast density from mammographic x-ray spectra using a cadmium telluride photon counting detector," *Med. Phys.* in press (2017).
12. K. Clark et al., "The cancer imaging archive (TCIA): maintaining and operating a public information repository," *J. Digital Imaging* **26**, 1045–1057 (2013).

Andreu Badal is a researcher at the US Food and Drug Administration. He received his PhD from the Universitat Politecnica de Catalunya in Barcelona, Spain, in 2008. He has a degree in physics from the Universitat de Barcelona in Barcelona, Spain. His main line of research is the development of x-ray imaging simulation software based on Monte Carlo methods.

Matthew Clark has a degree in mechanical engineering from the University of Maryland, College Park in 2017. He has a passion for 3D printing technology, and has worked in the development of an innovative 3D printer in a start-up company.

Bahaa Ghammraoui is a researcher at the US Food and Drug Administration. He received his PhD from the National Institute of Applied Sciences (INSA) in Lyon, France, in 2012, after obtaining his master's degree in interaction matter with radiation from Blaise Pascale University in Clermont Ferrand, France, in 2009. His primary research interest is the development of advanced x-ray based imaging techniques, especially for breast cancer diagnosis.